DEVELOPMENTAL NEUROSCIENCE

Pyramidal neuron growth and increased hippocampal volume during labor and birth in autism

R. Cloarec[1]*, B. Riffault[1]*, A. Dufour[1]*, H. Rabiei[1], L.-A. Gouty-Colomer[1], C. Dumon[1], D. Guimond[1], P. Bonifazi[2], S. Eftekhari[1], N. Lozovaya[1], D. C. Ferrari[1], Y. Ben-Ari[1]†

We report that the apical dendrites of CA3 hippocampal pyramidal neurons are increased during labor and birth in the valproate model of autism but not in control animals. Using the iDISCO clearing method, we show that hippocampal, especially CA3 region, and neocortical volumes are increased and that the cerebral volume distribution shifts from normal to lognormal in valproate-treated animals. Maternal administration during labor and birth of the NKCC1 chloride transporter antagonist bumetanide, which reduces $[Cl^-]_i$ levels and attenuates the severity of autism, abolished the neocortical and hippocampal volume changes and reduced the whole-brain volume in valproate-treated animals. These results suggest that the abolition of the oxytocin-mediated excitatory-to-inhibitory shift of GABA actions during labor and birth contributes to the pathogenesis of autism spectrum disorders by stimulating growth during a vulnerable period.

INTRODUCTION

Birth is among the most complex biological mechanisms in mammals, with major and abrupt hormonal, physiological, immunological, microbiotal, and vascular changes. It is associated with a massive release of stress molecules and hormones, including oxytocin required to trigger labor and mother-infant interactions and to compensate for the potentially deleterious actions of stress (*1*). Astonishingly, we have little information on how the brain is prepared for and endures this critical step. Several indirect lines of evidence obtained in humans suggest that brain growth velocity slows during the third trimester, possibly in an effort to avoid an exacerbated brain volume during vaginal delivery (*2*). This is followed by a spurt of growth after birth that correlates with synapse density (*3*). Despite their importance, human epidemiological investigations fall short in determining the nature of the events occurring during labor and birth. To understand whether and how the brain is prepared to meet that challenge, experimental studies comparing brain and neuronal parameters shortly before and after birth are essential. Gaining a better understanding of the cellular events occurring during labor and birth is also important from a clinical and public health perspective. Thus, epidemiological studies suggest higher incidence of autism spectrum disorders (ASD) and other developmental disorders following birth-related alterations, including C-sections (*4*), preterm delivery (*5*), or delivery complications (*6*). Experimental observations also suggest that labor and birth are critical periods, playing an important role in the pathogenesis of brain disorders (*7*).

Here, we compared neuronal morphology and brain volume shortly before and after birth in control (CTL) animals and observed that they are similar, suggesting a "growth stop signal" in preparation for labor and birth. We then tested the hypothesis that this stop signal is alleviated by intrauterine injections of valproate (VPA) in a timed pregnant rat. In this model, we observed a growth during the same short period. We showed that hippocampal neuronal morphology and cerebral volumes, including in the hippocampus and neocortex, were increased by labor and birth in ASD conditions. The NKCC1 chloride importer antagonist bumetanide, which attenuates ASD severity in children (*8*) and animal models of ASD (*9*, *10*), reduced some of these changes, suggesting that high levels of chloride during labor and birth are pathogenic.

RESULTS

CA3 pyramidal neuronal growth is altered in the VPA condition

Using a rat model of ASD by injection in utero of VPA (*9*), we first reconstructed CA3 hippocampal pyramidal cells. These neurons have been extensively investigated during the perinatal period to determine electrical and behavioral features of ASD (*9*, *11*). Referring to birth as the period between embryonic day 21 (E21) and the first postnatal day P0 (~24 hours) that includes labor and birth, we compared E21 CTL versus E21 VPA, E21 CTL versus P0 CTL, E21 VPA versus P0 VPA, and P0 CTL versus P0 VPA conditions (table S1). Despite a high degree of heterogeneity (Fig. 1, A to D, and figs. S1 and S2), we found no significant differences between E21 and P0 CTL neurons in all parameters investigated (Fig. 1, E to I, and fig. S3, A to C). There was a trend for E21 VPA neurons to be smaller than E21 CTL neurons but without reaching statistical significance, except for the Sholl profile (Fig. 1E). On the other hand, the Sholl profile of P0 VPA neurons was shifted to higher values [E21 CTL versus E21 VPA ($P < 0.0001$), E21 CTL versus P0 CTL ($P = 0.0684$), E21 VPA versus P0 VPA ($P < 0.0001$), and P0 CTL versus P0 VPA ($P = 0.0163$), Kolmogorov-Smirnov test; Fig. 1E]. In P0 VPA neurons, the total apical dendrite length (Fig. 1F), enclosing radius (Fig. 1G), and critical radius (Fig. 1H) were significantly higher compared with those in P0 CTL [$P = 0.0156$, 0.0110, and 0.0079, respectively; Kruskal-Wallis tests followed by Dunn's posttests (KWD)] and E21 VPA ($P < 0.0001$, $P < 0.0001$, and $P = 0.0004$, respectively, KWD). However, the number of apical nodes (Fig. 1I) was not different from P0 CTL or E21 VPA, indicating that the apical arbor complexity remained unchanged. Soma volumes were also significantly increased in P0 VPA compared with E21 VPA ($P = 0.0027$, KWD;

[1]Neurochlore, Ben-Ari Institute of Neuroarcheology (IBEN), Zone Luminy Biotech Entreprises, 13288 Cedex 09 , Marseille, France. [2]Biocruces Health Research Institute, Barakaldo, Spain & IKERBASQUE: The Basque Foundation for Science, Bilbao, Spain.
*These authors contributed equally to this work.
†Corresponding author. Email: ben-ari@neurochlore.fr

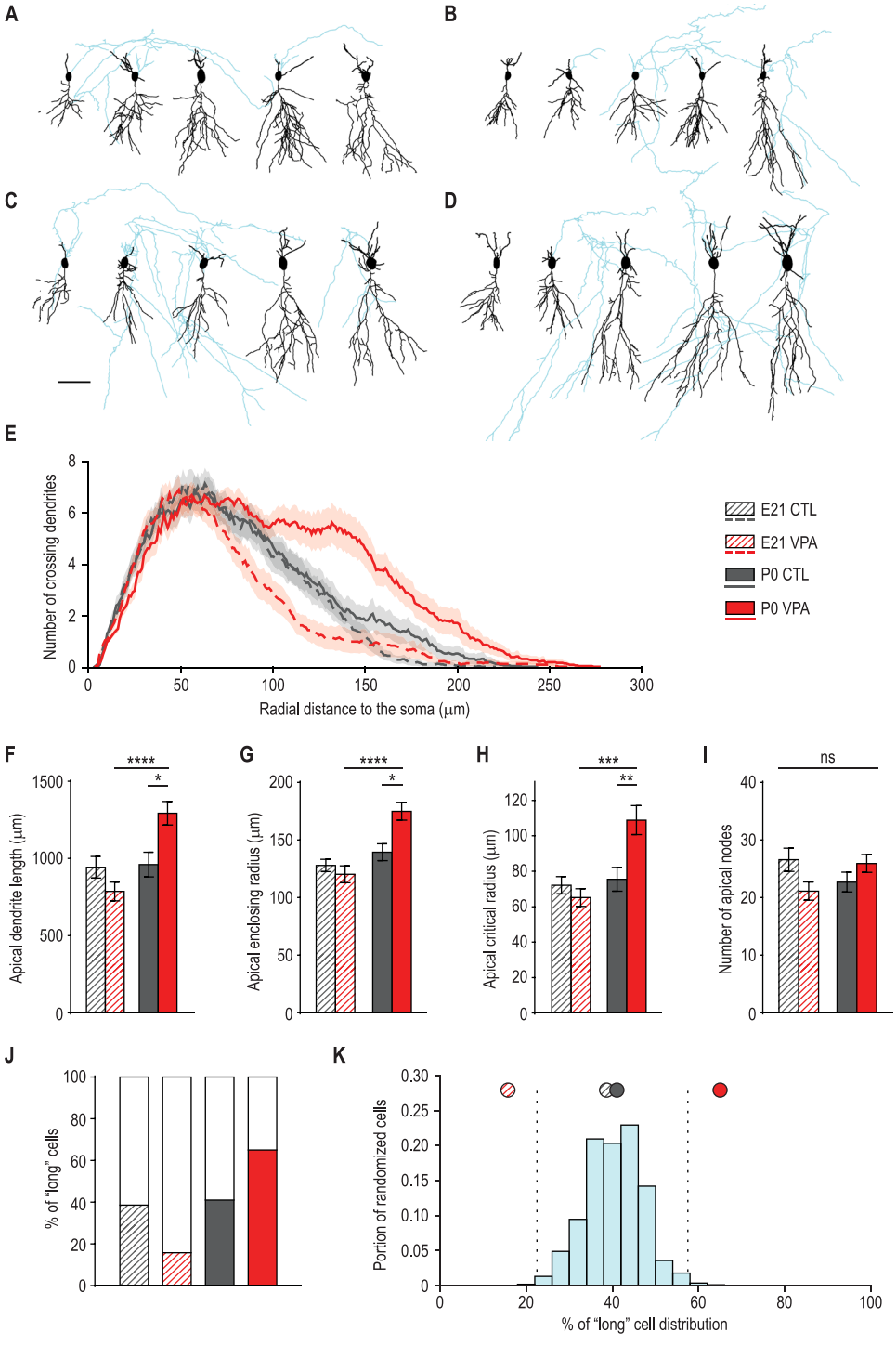

Fig. 1. CA3 pyramidal neuron morphology is affected during birth in the VPA condition. (**A** to **D**) Representative neuron reconstructions from E21 CTL (A), E21 VPA-treated (B), P0 CTL (C), and P0 VPA-treated (D) rats; axons are presented in blue. Scale bar, 50 μm. (**E**) Sholl profiles of apical dendrites illustrating shifts in the number of crossing dendrites along the radial axe occurring in the VPA conditions. (**F** to **I**) Mean values for the total apical dendrite length (F), the apical dendrite enclosing radius length (G), the apical dendrite critical radius (H), and the number of apical dendrite nodes (I). Error bars denote SEM. Kruskal-Wallis test followed by Dunn's posttest, $^{*}P < 0.05$, $^{**}P < 0.01$, $^{***}P < 0.001$, and $^{****}P < 0.0001$. ns, not significant ($P > 0.05$). (**J** and **K**) Long versus short cell clustering based on apical morphology. (J) Percentage of neurons distributed in the long cell cluster (the short cell cluster proportion is shown in white bars on top) for each condition. (K) Histogram showing the distribution of the long cell cluster proportion in 1000 randomizations of cell affiliation among all conditions where E21 and P0 VPA are found out of the range of possibilities for CTL conditions. Dashed lines indicate the 99% confidence interval.

fig. S3A), but the basal dendritic length and nodes as well as the number of basal dendrites were not different in any conditions (fig. S3, B and C). The sexual dimorphism reported in pyramidal cell morphology during late postnatal development (*12*) or adulthood (*13*) was not observed around birth (table S2). We then performed a cluster analysis based on apical morphological parameters (table S1). Pyramidal neurons were subdivided into "short" and "long" cell clusters and then reaffiliated to their age and condition. For E21 and P0 CTL, 38.64 and 41.02% of the cells were labeled long. The proportion of long cells was reduced in E21 VPA (15.79%) and increased in P0 VPA (65%; Fig. 1J). Randomization processes of cell affiliation among all conditions revealed that E21 and P0 VPA neurons were different from CTLs in proportions that differed from the range of random possibilities (Fig. 1K). Note that we excluded the influence of neuron location inside the CA3 region from the results (fig. S3, D to F). Collectively, these observations suggest that birth is associated with an abrupt increase of CA3 pyramidal neuron size in VPA-treated rats.

Microglia do not undergo major alterations during birth

Converging evidence from many studies suggests an involvement of microglia in neurodevelopmental disorders including autism (*14*). Since microglia can affect progenitor cell proliferation and neuronal growth during brain development (*15*), we assessed if these cells could be affected during birth in CTL and VPA animals. Using the iDISCO clearing method (*16*), we counted, for each condition, the total number and computed the density of IBA1 immunolabeled cells before and after birth for each condition in four different structures, including the hippocampus, neocortex, dorsolateral striatum, and whole brain (movie S1 and table S3). In CTL and VPA pups, the densities of microglia in these structures were similar before and after birth (Fig. 2, A and C, and fig. S4, A and B). Microglia activation state was then evaluated on the basis of the cellular area and volume (table S3) (*17*). Despite a significant reduction of hippocampal microglia activation in P0 VPA animals compared with P0 CTL [area, P0 CTL versus P0 VPA ($P = 0.0182$); volume, P0 CTL versus P0 VPA ($P = 0.0193$); KWD], we observed no differences in other brain structures for each condition (Fig. 2, B and D). Together, these results demonstrate that only hippocampal microglia activation state is affected in VPA neonates, suggesting a potential effect of VPA linked to birth. However, to which extent these cells might contribute to the CA3 neuronal growth remains to be clarified.

Volumetric alterations around birth in the VPA condition

Toddlers, children, and adolescents with ASD have bigger brains than normotypic ones (*18*–*20*), but whether these changes occur around birth is not known. To evaluate this, we used the same clearing method to compare, before and after birth, the volume of the hippocampus, neocortex, dorsolateral striatum, lateral ventricles, and whole brain in CTL and VPA-treated rats (movie S2 and table S4). In CTL rats, these volumes were not significantly different before and after birth [hippocampus, E21 CTL versus P0 CTL ($P > 0.9999$); neocortex, E21 CTL versus P0 CT ($P = 0.7944$); whole brain, E21 CTL versus P0 CTL ($P > 0.9999$); dorsolateral striatum, E21 CTL versus P0 CTL ($P > 0.9999$); and lateral ventricle, E21 CTL versus P0 CTL ($P > 0.9999$); KWD] [Fig. 3 (A and B) and figs. S4 (C and D), S5, and S6]. In contrast, major alterations were observed in VPA animals. The hippocampal and neocortical volumes were significantly bigger after birth than before [hippocampus, E21 VPA versus P0 VPA ($P = 0.0061$); neocortex, E21 VPA versus P0 VPA ($P < 0.0001$); KWD] (Fig. 3, A and B), suggesting a marked volume increase of these structures during birth. E21 VPA brains were significantly smaller than E21 CTLs [whole brain, E21 CTL versus E21 VPA ($P = 0.0241$); KWD] (Fig. 3, A and B). Also, there was a trend for the hippocampus, neocortex, and striatum to be smaller in E21 VPA animals compared with E21 CTL, but without reaching statistical significance. In contrast, the lateral ventricles were significantly smaller before and after birth in the VPA condition compared with CTLs, suggesting that the brain volume changes are not due to bigger ventricles [E21 CTL versus E21 VPA ($P = 0.0172$) and P0 CTL versus P0 VPA ($P < 0.0001$); KWD] (fig. S6). In keeping with this, after birth, the neocortex, hippocampus, and whole-brain volumes of CTL and VPA were similar, suggesting that the VPA structures go back to the reduced volumes they had before birth. Comparing E21 VPA and P0 VPA revealed that the neocortex and hippocampus were significantly bigger after birth, suggesting a marked volume increase of these structures during birth in the ASD condition.

To further examine differences between CTL and VPA, we compared the volume distributions of all the structures grouped together before and after birth. In CTL conditions, the cerebral volumes followed a normal distribution that was confirmed by the Shapiro-Wilk test of normality. In contrast, in the VPA condition, the distribution shifted from normal at E21 to lognormal after birth, with a right skewed form with large volumes far from the sample mode, validating the important volumetric changes occurring during birth in VPA brains (Fig. 3C).

A local shape analysis of hippocampal volumes was then performed to determine whether specific regions of that structure were affected by birth (Fig. 3D). The CA3 region was significantly smaller in E21 VPA compared with P0 VPA, but there was no difference between E21 and P0 CTL conditions, suggesting a significant increase of the CA3 region during birth in the VPA condition in accordance with the abrupt neuronal growth observed in the same region.

Maternal bumetanide treatment prevents the overgrowth in the VPA condition

Brief maternal administration of bumetanide before birth restores low neuronal intracellular chloride concentration ($[Cl^-]_i$) levels, produces an excitatory-to-inhibitory shift in the action of γ-aminobutyric acid (GABA), and attenuates the severity of electrical and behavioral features of ASD (*9*, *10*), suggesting that $[Cl^-]_i$ levels during birth might play an important role in the pathogenesis of ASD (*7*). Here, the same bumetanide treatment significantly reduced the hippocampal and neocortical volumes of P0 VPA pups, abolishing the volume increase observed during birth in the VPA condition [hippocampus: P0 VPA versus P0 VPA + BUM ($P = 0.0116$); neocortex: P0 VPA versus P0 VPA + BUM ($P = 0.0242$); KWD] (Fig. 3B). Maternal bumetanide treatment also shifted the distribution of cerebral volumes from lognormal back to normal in the population of VPA brains, restoring smaller cerebral structure volumes (Fig. 3C). It also decreased the CA3 volume to CTL level after birth, suggesting that the increased growth observed in this region could be mediated by the excitatory actions of GABA (Fig. 3D). Therefore, maternal bumetanide administration prevents the enhanced growth observed in VPA animals during birth.

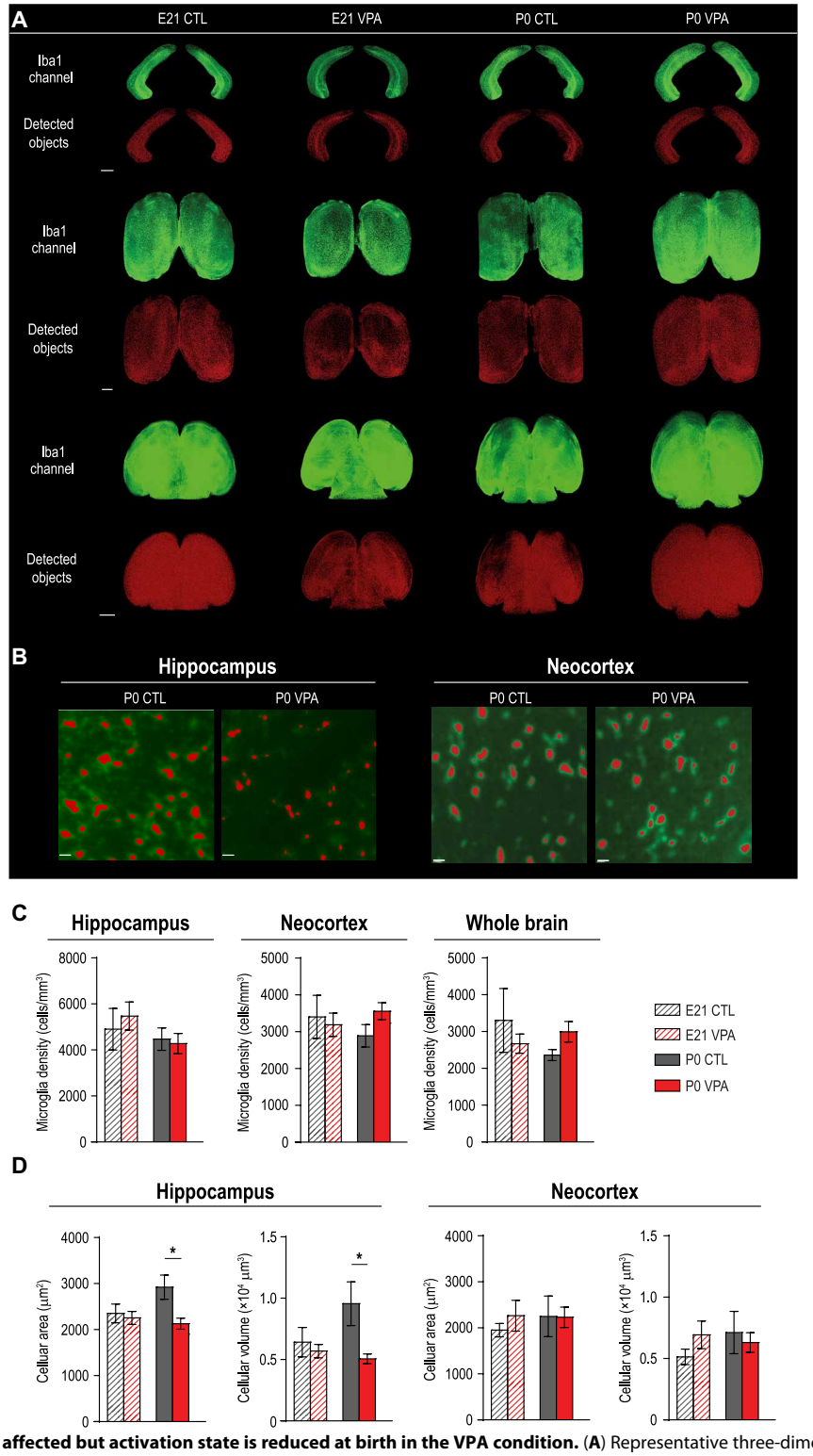

Fig. 2. Microglia density is not affected but activation state is reduced at birth in the VPA condition. (**A**) Representative three-dimensional (3D) pictures of hippocampal (top), neocortical (middle), and whole-brain (bottom) Iba1 immunoreactive cells (in green) and of automatically detected objects (in red) for E21 CTL, E21 VPA, P0 CTL, and P0 VPA conditions. Scale bars, 600 µm. (**B**) Representative pictures of morphometric-based analysis of hippocampal and neocortical microglia. An alteration of global cellular morphology (including soma and part of the branching processes) is visible in the hippocampus in the P0 VPA group compared with the CTL group, compatible with a reduced activation state. Iba1, green; detected surfaces superimposed, red. Scale bars, 100 µm. (**C**) Hippocampal, neocortical, and the whole-brain quantification showing no alterations of microglia density (number of cells per mm^3) in VPA animals compared with the CTL ones. (**D**) In the hippocampus, VPA treatment induces a significant decrease of microglial area and volume parameters at birth, correlated with a reduced activated state of these cells. Error bars denote SEM. Kruskal-Wallis test followed by Dunn's posttest, *$P < 0.05$.

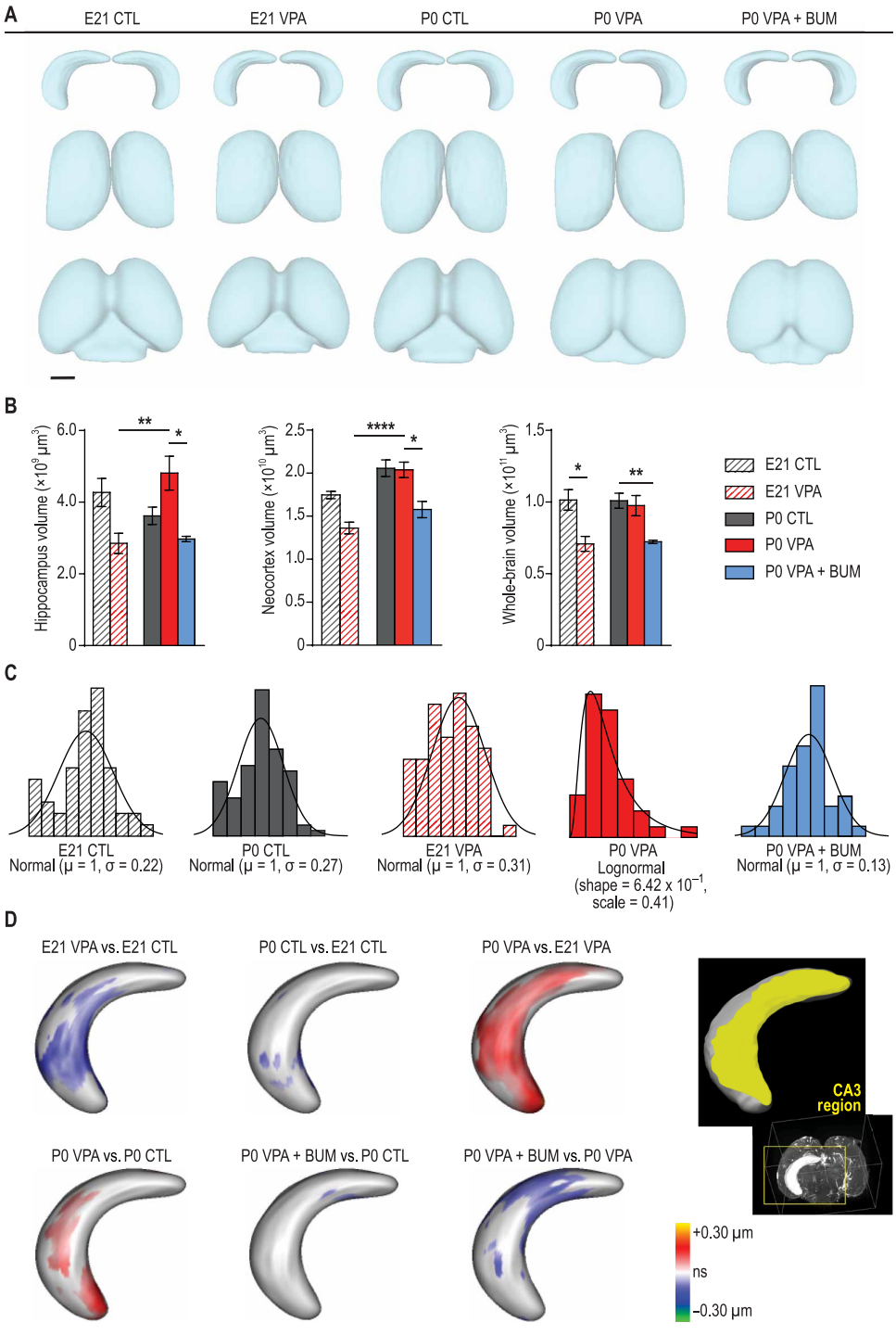

Fig. 3. VPA treatment induces volumetric alterations of the hippocampus, whole brain, and neocortex around birth. (**A**) Average shape of the hippocampus (top), neocortex (middle), and whole brain (bottom) for E21 CTL, E21 VPA, P0 CTL, P0 VPA, and P0 VPA + BUM conditions. Scale bar, 1 mm. (**B**) Volume measurements of the hippocampus, neocortex, and whole brain. Error bars denote SEM. Kruskal-Wallis test followed by Dunn's posttest, $*P < 0.05$, $**P < 0.01$, and $****P < 0.0001$. ns, not significant ($P > 0.05$). (**C**) Distribution of normalized volumes of all structures in each experimental group. After birth in the VPA group, the distribution is changed to lognormal, and normal law is restored by bumetanide. (**D**) Representation of significant local size changes between groups of interest. Kruskal-Wallis test followed by Dunn's posttest ($P < 0.05$, corrected with the Benjamini-Hochberg procedure for multiple comparisons). Red-yellow colors show significant size increase, blue-green colors indicate significant size decrease, and gray color is assigned to regions with nonsignificant size changes. Representative segmented CA3 region in yellow (right).

DISCUSSION

Neuronal and brain "growth stop signal" in preparation to birth

To the best of our knowledge, this is the first description of global brain changes around birth in CTL and in an ASD rodent model. Birth being one of the most complex biological mechanisms in mammals, it is intuitively expected that some alterations in brain functions occur in preparation for it. Yet, despite its importance, our knowledge of the events occurring shortly before and after birth is very limited. Volumetric fluorescence macroimaging of whole organs provides a new approach to study how tissues and cells develop and respond to disease. In CTL rats, there is no difference between shortly before and after birth, indicating that brain growth is halted or at least does not occur during that period. We also show that CA3 pyramidal neuron apical dendrites and somata are similar at E21 and P0. The volume of structures, including the hippocampus, neocortex, and striatum, is also unaltered, suggesting a common sequence. Astonishingly, the ventricle volumes are increased. More investigations are much needed to determine whether a given structure possibly indispensable for the functions that must be executed at birth (crawling, suction, and smell) might not show this lack of growth during this period.

Intrauterine VPA abolishes the growth stop signal during birth

In the VPA condition, CA3 pyramidal neurons in offspring at birth had longer apical dendrites and bigger somata but showed no changes in basal dendrites. The volumes of the hippocampus and neocortex were also significantly increased, but not the lateral ventricles, in contrast to CTLs, suggesting major changes of the neuropil during birth. Major morphological alterations have been reported in animal models and postmortem investigations in patients with ASD. Thus, in the VPA rat model, dendritic arborization of neurons in layer 2 of the motor cortex is more complex than in CTL condition (*21*). Following intrauterine VPA, the number of spines is reduced in the hippocampus, the prefrontal cortex, and the basolateral amygdala but increased in the nucleus accumbens and layer 3 of the prefrontal cortex (*22*). Maternal immune activation that is associated with increased incidence in ASD also leads to profound cortical malformations that are the direct cause of the deleterious social impairments (*23*, *24*). Postmortem studies in children with ASD (2 to 15 years old) revealed focal patches of abnormal laminar cytoarchitecture and cortical disorganization of neurons (*25*). Individuals with ASD show at birth an initial excess of mature neurons (*26*). Similarly, neuron number in the prefrontal cortex was increased by 67% in children with ASD (2 to 16 years old), and brain weight was bigger than in age-matched CTLs (*27*). Collectively, these studies suggest that the variety of events leading to ASD also lead to morphological cortical abnormalities. In addition, children with ASD have a bigger brain (*28*, *29*). Thus, 15% of boys with ASD have megalencephaly, with a brain size that is disproportionate to the body (*18*). Also, brain imaging functional connectivity differs already at 6 months of age in babies with ASD (*30*). The brains of children with ASD undergo an abnormal brain trajectory that includes a period of overgrowth (*28*). The authors suggest that the enlargement starts at the end of the first postnatal year, but direct evidence on this issue is lacking. Neither the earlier occurrence of these changes nor whether birth constitutes a flag point in this sequence is understood at this time. Present results suggest that bigger brain structures and enhanced neuronal growth are conspicuous early on and that at least in the VPA model, neurons grow and brain structures increase their volumes during birth. The intrauterine insults by a not yet understood mechanism inactivate a putative neuroprotective mechanism occurring during this vulnerable period.

Bumetanide-sensitive excitatory GABA and growth during birth in the VPA condition

The reduction of the volume changes produced in offspring by maternal bumetanide suggests that GABAergic signals and, notably, neuronal $[Cl^-]_i$ levels might contribute to these volume changes. The volumes of the hippocampus, neocortex, and lateral striatum were not increased after treatment, in contrast to CTLs. GABA exerts a trophic action on development, including cell proliferation (*31*), neuronal migration (*32*), differentiation (*33*), network formation (*34*, *35*), and dendritic growth (*36*–*39*). This phenomenon is mediated by the excitatory actions of GABA that activate voltage-gated calcium currents and increase intracellular calcium levels, releasing growth factors, notably BDNF (brain-derived neurotrophic factor), that modulate neuronal growth and dendritic extension (*40*, *41*). These effects are mediated by the high $[Cl^-]_i$ levels present in immature neurons and require active NKCC1 chloride import, as they are blocked by the highly specific antagonist bumetanide or by NKCC1 shRNA (short hairpin RNA) manipulations to invalidate the importer (*37*, *39*, *42*). Furthermore, in human and mice embryos, there is a depolarizing GABAergic projection from the zona incerta to cortical layer 1 that stimulates dendritic growth from deeper cortical layers, and silencing this activity decreases dendritic growth (*38*). Therefore, high $[Cl^-]_i$ levels and excitatory actions of GABA are indispensable for embryonic neuronal growth.

However, during birth, this excitatory action might exert potentially deleterious actions. Birth is associated with a massive release of stress molecules (*43*) that augment $[Cl^-]_i$ levels, leading to neuronal hyperexcitability and potential seizures during a highly vulnerable period (*44*, *45*). Oxytocin induces during birth an abrupt depolarizing-to-hyperpolarizing shift of GABA actions associated with a reduction of $[Cl^-]_i$ levels exerting an antistress action (*11*). This phenomenon was abolished in the VPA model of ASD and in fragile X mice (*9*) but was restored by maternal administration of bumetanide during birth, which also attenuated the severity of ASD (*9*, *10*). Here, we show that bumetanide possibly restores the brain growth stop signal, suggesting that the high $[Cl^-]_i$ levels during this critical period are instrumental in the long-term deleterious sequelae of ASD. Bumetanide attenuates ASD severity in children and adolescents (*8*).

Therefore, the neuroprotective oxytocin-mediated mechanism is alleviated in the VPA model of ASD; GABA depolarizes and excites neurons leading to growth factor release, neuronal growth, and enhanced hippocampal and neocortical volumes. Growth during labor and birth might underlie the defects in neuronal and network wiring and affect an essential period of sensory acquisition and social interactions. Birth itself acts as a triggering signal to accelerate cortical sensory maps and major early functions including suction (*46*, *47*). It is suggested that the reduction of the inhibitory actions of GABA and the aberrant synchronized activity generated consequently affect this operation, leading to long-term sequelae.

CONCLUSION

Despite the intrinsic limitations of species differences, our results stress the need to consider birth as a critical period in the pathogenesis of ASD (*7*). The present approach provides means to compare genetic or environmental intrauterine insults and determine common rules between different disorders.

MATERIALS AND METHODS

VPA rat model of autism

All experiments were performed in accordance with the European Community Council directives regarding the protection of animals used for experimental and scientific purposes (2010/63/EU).

Time-mated female Wistar rats, housed under standard laboratory conditions, were treated by in utero VPA injection to generate ASD in offspring (*9*). Briefly, the sodium salt of VPA (Sigma-Aldrich Inc., USA) was dissolved in physiological saline solution to a concentration of 300 mg/ml. Pregnant rats received a single intraperitoneal dose of 600 mg/kg on gestational day 12 (E12). CTL animals were not manipulated. In our laboratory conditions, the day of delivery was on E22, without differences between CTL and VPA-treated females. Bumetanide treatment (2 mg/kg; Sigma-Aldrich) was given to the dams in drinking water at least 12 hours before birth. The offspring were used for experiments on E21 and postnatal day 0 (P0 = E22). Experiments were performed on animals of both sexes. E21 embryos were extracted from the dams by hysterectomy after isoflurane anesthesia (Aerrane, Baxter, France), followed by cervical dislocation. Newborn P0 pups were decapitated shortly after delivery. For morphology, brains were immediately placed in an ice-cold oxygenated solution for slicing. For iDISCO experiments, brains were postfixed in Antigenfix (Diapath, Italy) for overnight fixation and stored at 4°C in phosphate buffer containing 0.9% NaCl [phosphate-buffered saline (PBS), Thermo Fisher Scientific Inc., USA] with 0.05% sodium azide (Sigma-Aldrich) until use. For each embryo and pup, a biopsy of the tail was kept for sex genotyping (chromosome Y). Morphology and iDISCO experiments were performed blindly.

Slice preparation and revelation processing of biocytin-filled pyramidal neurons

We prepared horizontal brain slices (350 µm thick) from E21 and P0 male and female rats using a Leica VT1200 S (Leica Microsystems, Germany) vibratome in ice-cold oxygenated solution containing 132.5 mM choline chloride, 2.5 mM KCl, 1.23 mM NaH_2PO_4, 3 mM $MgCl_2$, 0.7 mM $CaCl_2$, 25 mM $NaHCO_3$, and 8 mM glucose. Slices were then left to recover for 1 hour at room temperature (22° to 25°C) in artificial cerebrospinal fluid containing 126 mM NaCl, 3.5 mM KCl, 1.2 mM NaH_2PO_4, 2 mM $CaCl_2$, 1 mM $MgCl_2$, 11 mM glucose, and 25 mM $NaHCO_3$ (pH 7.4). All solutions were bubbled with 95% O_2/5% CO_2. Borosilicate glass pipettes (4 to 7 megohm) were filled with a solution containing 130 mM K-gluconate, 10 mM Na-gluconate, 7 mM NaCl, 4 mM Mg–ATP (adenosine 5′-triphosphate), 10 mM Hepes, 4 mM phosphocreatine, and 0.3 mM Na–GTP (guanosine 5′-triphosphate) (pH 7.3) with KOH , 285 to 290 mOsm. Biocytin (0.5 to 1%; Sigma-Aldrich) was added to the solution just before patching the cells.

After biocytin diffusion into the cells (10 min), slices were transferred into Antigenfix for overnight fixation. Aldehyde fixation causes nonuniform brain tissue shrinkage (*48*), making it very difficult to apply any correction factor. Thus, special care was taken to respect the exact equal time of fixation and processing for each slice to decrease, as much as possible, the shrinkage variability (*49*).

After fixation, slices were sequentially washed in PBS, 0.3M glycine in PBS, and PBS. They were incubated for 1 hour at room temperature in PBS containing 10% of normal goat serum (NGS; Jackson ImmunoResearch Inc., USA), 1% bovine serum albumin (BSA; Sigma-Aldrich), and 0.3% of Triton X-100 (Sigma-Aldrich). They were then incubated overnight at 4°C, with streptavidin coupled with Alexa 647 (1/1000; Thermo Fisher Scientific Inc., USA) diluted in PBS containing 1% NGS and 1% BSA and 0.3% of Triton X-100. CTL slices without any biocytin were systematically added in each experiment to check the streptavidin specificity. Last, slices were washed in PBS and incubated for 10 min at room temperature with Hoechst staining solution (1/1000; Sigma-Aldrich) diluted in PBS. They were washed in PBS, mounted on slides, and coverslipped using Fluoromount-G (Electron Microscopy Sciences, USA) as mounting medium.

Image acquisition and morphology analyses

Confocal images were acquired on an SP5X Leica microscope (Leica Microsystems) using the 647-nm band of a white laser for excitation of Alexa 647 (spectral detection, 657 to 750 nm) and a diode 405 nm for excitation of Hoechst staining (spectral detection, 411 to 479 nm). High-magnification images (1024 × 1024 pixel) of Alexa 647 signal were acquired at 200 Hz using a 63× oil immersion objective, pinhole set to "Airy 1." Stacks for dendrite analysis were obtained by scanning with a line average of 2 and a *z* step of 0.50 µm.

Morphology analyses were blindly performed to avoid any bias. Neurons were selected according to their localization in the stratum pyramidale of CA3 and the quality of their staining; dying cells, damaged cells, and interneurons were systematically excluded. Patches were done in the entire CA3 area to guaranty homogeneity in cell origins between ages and conditions. Thus, similar proportions of cells were found localized in the CA3a, b versus CA3c subregions (less than 4% of difference; fig. S3D). The position of each cell was noted, as it was shown that CA3a, b, and c exhibit a gradient in pyramidal cell morphology (*50*). Somata depth positions inside the stratum pyramidale were also carefully noted. In juvenile and adult rodents, deep pyramidal cells (near stratum oriens) are known to be older and longer than superficial neurons [near stratum lucidum/radiatum; (*51*, *52*)].

For dendrite and somata analysis, stacks were imported in the open-source platform Fiji (1.50e, Java 1.8.0_60, 64 bit; https://fiji.sc/) and stitched together (https://imagej.net/Image_Stitching). Without any additional preprocessing, somata reconstruction was performed using the ROI manager tool, and dendrite reconstruction and measurements were performed using the semiautomatic "Simple Neurite Tracer" plugin (http://imagej.net/Simple_Neurite_Tracer). On the basis of the reconstructions, a Sholl analysis of apical dendrites was then performed using the "Sholl Analysis" plugin (http://imagej.net/Sholl_Analysis). Apical morphological parameters (table S1) were also used to perform a cluster analysis.

K-means clustering was performed in MATLAB (Mathworks Inc., USA) using Euclidean distance, 100 times iterations and 100 times replicates. Clustering was aimed at creating two clusters of cells based on the six following morphological properties (variables): total apical dendrite length, apical dendrite nodes, apical primary dendrite length, ending radius, critical radius, and maximum crossing dendrites. Each variable was normalized by its own maximum, with

resulting values between 0 and 1. In each cluster, the average total apical dendrite length was used as reference to identify the cluster with longer and the one with shorter average total apical dendrite length. To create a surrogate statistic on the clustering analysis, the group labeling of the cells (i.e., E21 CTL, E21 VPA, P0 CTL, and P0 VPA) was reassigned randomly between the list of cells while keeping the same number of cells per group. The same clustering procedure was then performed over 10,000 surrogate cell lists, and the distribution of the cells in each cluster (long versus short neurons) per group was calculated so that a 99% confidence interval could be estimated.

iDISCO protocol

Whole-brain clearing was performed according to the previously reported 3DISCO and iDISCO+ clearing procedures (*16*, *53*, *54*) with slight modifications. Samples were dehydrated in a graded series (20, 40, 60, 80, and 100%) of methanol (Sigma-Aldrich) diluted in PBS during 1.5 hours each, at room temperature. They were then incubated overnight at room temperature on a platform shaker in a solution of PBSG-T [PBS containing 0.2% gelatin (Sigma-Aldrich), 0.5% Triton X-100, 0.02% sodium azide (Sigma-Aldrich)] for 2 days. Next, samples were transferred to PBSG-T containing Iba1 primary antibody (1:500; rabbit anti-Iba1, Wako Chemicals Inc., USA) to label microglia and placed at 37°C, with rotation at 100 rpm, for 10 days. This was followed by six washes of 1 hour in PBSG-T at room temperature. Samples were then incubated in secondary antibody (donkey anti-rabbit Alexa 647) diluted in PBSG-T for 2 days at 37°C. After six washes of 1 hour in PBSG-T at room temperature, samples were stored at 4°C in PBS until use. For tissue clearing, all incubation steps were performed at room temperature using a 15-ml polypropylene tube (Dutscher SAS, France) covered with aluminum foil to avoid exposure to light. Samples were dehydrated in a graded series (20, 40, 60, 80, and 100%) of methanol diluted in PBS during 1 hour. This was followed by a delipidation step of 20 min in dichloromethane (DCM; Sigma-Aldrich). Samples were then transferred to 100% DCM until they have sunk. Last, samples were cleared overnight in dibenzylether (DBE; Sigma-Aldrich) and stored in DBE at room temperature in the dark.

iDISCO imaging and image processing

Three-dimensional (3D) imaging was performed with an ultramicroscope (LaVision BioTec GmbH, Germany) using ImspectorPro software (LaVision BioTec). The light sheet was generated by a laser (wavelengths, 488, 555, and 647 nm; Coherent Sapphire Laser, LaVision BioTec) and two cylindrical lenses. A binocular stereomicroscope (MXV10, Olympus, Japan), with a 2× objective (MVPLAPO, Olympus), was used at magnification ×2.5. Samples were placed in an imaging tank made of 100% quartz (LaVision BioTec) filled with DBE and illuminated from the side by the laser light. Images were acquired with a pco.edge sCMOS charge-coupled device camera (2560 × 2160 pixel size, LaVision BioTec). The step size between each image was fixed at 2 µm. 3D image quantifications were generated using Imaris x64 software (version 9.2.1, Bitplane, Switzerland). Each resulting Imaris file was 16-bit images and was subsequently converted to 8 bits. A 3D reconstruction of each sample was performed using the volume rendering tool (Imaris). Segmentation-based tracing of the whole brain, neocortex, hippocampus, dorsolateral striatum, and lateral ventricules was performed using the Imaris "Surface" module in manual creation mode. Border delineation of each structure was achieved on the autofluorescent channel generated by a 488-nm light exposure. Anatomical frontiers of each brain structure were followed according to the Allen Brain Atlas [Allen Institute (*55*)] and adapted to the developing rat brain. 3D pictures were generated using the "snapshot" tool (Imaris).

Image registration to compute average shapes of the whole brain, hippocampus, and neocortex was performed using a python script, MeshLab software (www.meshlab.net/), and the SPHARM module of 3DSlicer software (www.slicer.org/). First, the triangulation data of reconstructed surfaces were exported from Imaris. Then, the quality of mesh was checked by PyMesh library of python. When needed, we used MeshLab to modify the mesh quality and for visualization. Then, the surfaces in each group were registered using the SPHARM module. SPHARM establishes an optimized bijective mapping of each surface to the unit sphere. Consequently, for each point on a surface, corresponding points on other surfaces were specified. Last, surfaces were aligned on the basis of the first-order ellipsoid, and the average of each coordinate component was computed in python.

Morphometric analysis of microglia

Automated microglia cell detection was performed with the Imaris "spots" feature using an estimated *XY* diameter of 20 µm, and a threshold was applied on the basis of the intensity at the center of the spot, Gaussian filtered by 3/4 of spot radius, allowing an accurate detection of visible cells without including the background signal.

Measurement of microglia reactivity was performed according to previously reported work (*18*), which describes "resting" microglia as small with elaborate ramifications and the "activated" as bigger, more amoeboid cells with retracted processes. To quantitatively describe this morphological switch, we analyzed cell area and volume that are morphological parameters expected to be modified when cells become activated. This morphometric measurement of microglia activation was achieved with the Imaris "Surface" tool using a diameter of the largest sphere of 20 µm. Upper and lower thresholds of surface area and volume were determined as 3/2 of interquartile range below and above the first and third quartiles, respectively.

Local shape analysis

To investigate the local size changes of the hippocampus, the shortest distance of each point of every hippocampal surface to an individual medial axis, created by the SPHARM module through the hippocampus, was computed (fig. S7) (*56*). The intergroup comparisons of local distance maps in corresponding points were performed by using the Kruskal-Wallis test followed by post hoc Dunn's test ($P < 0.05$). The P values were corrected for multiple comparisons by using the Benjamini-Hochberg procedure. The significant local signed difference maps are shown in Fig. 3D.

Movie processing

Movies were generated using Imaris x64 software (version 8.0.1, Bitplane). Stack images were first converted to an Imaris file (.ims) using ImarisFileConverter, and the 3D reconstruction was performed using the "volume rendering" function. Optical slices were obtained using the "orthoslicer" tool. To isolate a specific region of the tissue, the surface tool was used and the mask option was selected. Movies were then generated using the "animation" tools. Movie reconstruction with .tiff series was done with Fiji, and addition of titles and transitions have been done with iMovie (version 10.1.9, Apple Inc., USA).

Statistics

Statistics were performed in Prism 6 (GraphPad Software Inc., USA). After checking normality using the Shapiro-Wilk test, multiple comparisons of parameters between each group were carried out using Kruskal-Wallis tests, followed by post hoc Dunn's tests. Sholl profiles were compared using the Kolmogorov-Smirnov test, male versus female parameter comparisons were made using the Mann-Whitney test, and correlation analyses were performed using the Spearman test since data were nonparametric. Exact *P* values were specified when possible and considered significant when <0.05. Results are shown as means ± SEM in tables S1 to S4. Images were edited using Photoshop CC and Illustrator CC (Adobe Systems Software Ireland Ltd., Ireland).

SUPPLEMENTARY MATERIALS

Supplementary material for this article is available at http://advances.sciencemag.org/cgi/content/full/5/1/eaav0394/DC1

Table S1. Morphological parameters based on dendrite reconstruction.
Table S2. Comparison of males (M) versus females (F) pyramidal cell morphology.
Table S3. Microglia number and density (per mm^3) and area (μm^2) and volume (μm^3).
Table S4. Volume quantifications (μm^3) for all brain structures.
Fig. S1. Reconstructions of CA3 pyramidal neurons of E21 and P0 CTL rats.
Fig. S2. Reconstructions of CA3 pyramidal neurons of E21 and P0 VPA-treated rats.
Fig. S3. Nonapical pyramidal cell morphology alterations and cell position within the CA3 zone.
Fig. S4. Effect of birth on microglia density and volume in the dorsolateral striatum of CTL and VPA-treated rats.
Fig. S5. The iDISCO clearing method enables concurrent 3D volume analyses of brains of rat pups.
Fig. S6. Lateral ventricle changes among all conditions (E21 CTL, E21 VPA, P0 CTL, P0 VPA, and P0 VPA + BUM).
Fig. S7. Medial axis and distance map of hippocampus.
Movie S1. Spot detection of hippocampal microglia and morphometric-based microglia analysis.
Movie S2. Imaris segmentation of all brain structures.

REFERENCES AND NOTES

1. R. Feldman, O. Golan, Y. Hirschler-Guttenberg, S. Ostfeld-Etzion, O. Zagoory-Sharon, Parent–child interaction and oxytocin production in pre-schoolers with autism spectrum disorder. *Br. J. Psychiatry* **205**, 107–112 (2014).
2. M. Fujimura, J. I. Seryu, Velocity of head growth during the perinatal period. *Arch. Dis. Child.* **52**, 105–112 (1977).
3. R. C. Knickmeyer, S. Gouttard, C. Kang, D. Evans, K. Wilber, J. K. Smith, R. M. Hamer, W. Lin, G. Gerig, J. H. Gilmore, A structural MRI study of human brain development from birth to 2 years. *J. Neurosci.* **28**, 12176–12182 (2008).
4. E. A. Curran, S. M. O'Neill, J. F. Cryan, L. C. Kenny, T. G. Dinan, A. S. Khashan, P. M. Kearney, Research review: Birth by caesarean section and development of autism spectrum disorder and attention-deficit/hyperactivity disorder: A systematic review and meta-analysis. *J. Child Psychol. Psychiatry* **56**, 500–508 (2015).
5. B. M. D'Onofrio, Q. A. Class, M. E. Rickert, H. Larsson, N. Långström, P. Lichtenstein, Preterm birth and mortality and morbidity: A population-based quasi-experimental study. *JAMA Psychiat.* **70**, 1231–1240 (2013).
6. T. D. Cannon, T. G. M. van Erp, I. M. Rosso, M. Huttunen, J. Lönnqvist, T. Pirkola, O. Salonen, L. Valanne, V.-P. Poutanen, C.-G. Standertskjöld-Nordenstam, Fetal hypoxia and structural brain abnormalities in schizophrenic patients, their siblings, and controls. *Arch. Gen. Psychiatry* **59**, 35–41 (2002).
7. Y. Ben-Ari, Is birth a critical period in the pathogenesis of autism spectrum disorders? *Nat. Rev. Neurosci.* **16**, 498–505 (2015).
8. E. Lemonnier, N. Villeneuve, S. Sonie, S. Serret, A. Rosier, M. Roue, P. Brosset, M. Viellard, D. Bernoux, S. Rondeau, S. Thummler, D. Ravel, Y. Ben-Ari, Effects of bumetanide on neurobehavioral function in children and adolescents with autism spectrum disorders. *Transl. Psychiatry* **7**, e1124 (2017).
9. R. Tyzio, R. Nardou, D. C. Ferrari, T. Tsintsadze, A. Shahrokhi, S. Eftekhari, I. Khalilov, V. Tsintsadze, C. Brouchoud, G. Chazal, E. Lemonnier, N. Lozovaya, N. Burnashev, Y. Ben-Ari, Oxytocin-mediated GABA inhibition during delivery attenuates autism pathogenesis in rodent offspring. *Science* **343**, 675–679 (2014).
10. S. Eftekhari, A. Shahrokhi, V. Tsintsadze, R. Nardou, C. Brouchoud, M. Conesa, N. Burnashev, D. C. Ferrari, Y. Ben-Ari, Response to Comment on "Oxytocin-mediated GABA inhibition during delivery attenuates autism pathogenesis in rodent offspring". *Science* **346**, 176 (2014).
11. R. Tyzio, R. Cossart, I. Khalilov, M. Minlebaev, C. A. Hübner, A. Represa, Y. Ben-Ari, R. Khazipov, Maternal oxytocin triggers a transient inhibitory switch in GABA signaling in the fetal brain during delivery. *Science* **314**, 1788–1792 (2006).
12. K. P. Keil, S. Sethi, M. D. Wilson, H. Chen, P. J. Lein, In vivo and in vitro sex differences in the dendritic morphology of developing murine hippocampal and cortical neurons. *Sci. Rep.* **7**, 8486 (2017).
13. J. M. Juraska, J. M. Fitch, D. L. Washburne, The dendritic morphology of pyramidal neurons in the rat hippocampal CA3 area. II. Effects of gender and the environment. *Brain Res.* **479**, 115–119 (1989).
14. C. A. Edmonson, M. N. Ziats, O. M. Rennert, A non-inflammatory role for microglia in autism spectrum disorders. *Front. Neurol.* **7**, 9 (2016).
15. K. M. Lenz, L. H. Nelson, Microglia and beyond: Innate immune cells as regulators of brain development and behavioral function. *Front. Immunol.* **9**, 698 (2018).
16. M. Belle, D. Godefroy, C. Dominici, C. Heitz-Marchaland, P. Zelina, F. Hellal, F. Bradke, A. Chédotal, A simple method for 3D analysis of immunolabeled axonal tracts in a transparent nervous system. *Cell Rep.* **9**, 1191–1201 (2014).
17. B. M. Davis, M. Salinas-Navarro, M. F. Cordeiro, L. Moons, L. De Groef, Characterizing microglia activation: A spatial statistics approach to maximize information extraction. *Sci. Rep.* **7**, 1576 (2017).
18. D. G. Amaral, D. Li, L. Libero, M. Solomon, J. Van de Water, A. Mastergeorge, L. Naigles, S. Rogers, C. Wu Nordahl, In pursuit of neurophenotypes: The consequences of having autism and a big brain. *Autism Res.* **10**, 711–722 (2017).
19. E. Courchesne, R. Carper, N. Akshoomoff, Evidence of brain overgrowth in the first year of life in autism. *JAMA* **290**, 337–344 (2003).
20. E. Courchesne, K. Pierce, C. M. Schumann, E. Redcay, J. A. Buckwalter, D. P. Kennedy, J. Morgan, Mapping early brain development in autism. *Neuron* **56**, 399–413 (2007).
21. W. M. Snow, K. Hartle, T. L. Ivanco, Altered morphology of motor cortex neurons in the VPA rat model of autism. *Dev. Psychobiol.* **50**, 633–639 (2008).
22. M. E. Bringas, F. N. Carvajal-Flores, T. A. López-Ramírez, M. Atzori, G. Flores, Rearrangement of the dendritic morphology in limbic regions and altered exploratory behavior in a rat model of autism spectrum disorder. *Neuroscience* **241**, 170–187 (2013).
23. G. B. Choi, Y. S. Yim, H. Wong, S. Kim, H. Kim, S. V. Kim, C. A. Hoeffer, D. R. Littman, J. R. Huh, The maternal interleukin-17a pathway in mice promotes autism-like phenotypes in offspring. *Science* **351**, 933–939 (2016).
24. Y. Shin Yim, A. Park, J. Berrios, M. Lafourcade, L. M. Pascual, N. Soares, J. Yeon Kim, S. Kim, H. Kim, A. Waisman, D. R. Littman, I. R. Wickersham, M. T. Harnett, J. R. Huh, G. B. Choi, Reversing behavioural abnormalities in mice exposed to maternal inflammation. *Nature* **549**, 482–487 (2017).
25. R. Stoner, M. L. Chow, M. P. Boyle, S. M. Sunkin, P. R. Mouton, S. Roy, A. Wynshaw-Boris, S. A. Colamarino, E. S. Lein, E. Courchesne, Patches of disorganization in the neocortex of children with autism. *N. Engl. J. Med.* **370**, 1209–1219 (2014).
26. T. A. Avino, N. Barger, M. V. Vargas, E. L. Carlson, D. G. Amaral, M. D. Bauman, C. M. Schumann, Neuron numbers increase in the human amygdala from birth to adulthood, but not in autism. *Proc. Natl. Acad. Sci. U.S.A.* **115**, 3710–3715 (2018).
27. E. Courchesne, P. R. Mouton, M. E. Calhoun, K. Semendeferi, C. Ahrens-Barbeau, M. J. Hallet, C. C. Barnes, K. Pierce, Neuron number and size in prefrontal cortex of children with autism. *JAMA* **306**, 2001–2010 (2011).
28. C. M. Schumann, C. S. Bloss, C. C. Barnes, G. M. Wideman, R. A. Carper, N. Akshoomoff, K. Pierce, D. Hagler, N. Schork, C. Lord, E. Courchesne, Longitudinal magnetic resonance imaging study of cortical development through early childhood in autism. *J. Neurosci.* **30**, 4419–4427 (2010).
29. H. C. Hazlett, H. Gu, B. C. Munsell, S. H. Kim, M. Styner, J. J. Wolff, J. T. Elison, M. R. Swanson, H. Zhu, K. N. Botteron, D. L. Collins, J. N. Constantino, S. R. Dager, A. M. Estes, A. C. Evans, V. S. Fonov, G. Gerig, P. Kostopoulos, R. C. McKinstry, J. Pandey, S. Paterson, J. R. Pruett, R. T. Schultz, D. W. Shaw, L. Zwaigenbaum, J. Piven; The IBIS Network, Early brain development in infants at high risk for autism spectrum disorder. *Nature* **542**, 348–351 (2017).
30. R. W. Emerson, C. Adams, T. Nishino, H. C. Hazlett, J. J. Wolff, L. Zwaigenbaum, J. N. Constantino, M. D. Shen, M. R. Swanson, J. T. Elison, S. Kandala, A. M. Estes, K. N. Botteron, L. Collins, S. R. Dager, A. C. Evans, G. Gerig, H. Gu, R. C. McKinstry, S. Paterson, R. T. Schultz, M. Styner; IBIS Network, B. L. Schlaggar, J. R. Pruett Jr., J. Piven, Functional neuroimaging of high-risk 6-month-old infants predicts a diagnosis of autism at 24 months of age. *Sci. Transl. Med.* **9**, eaag2882 (2017).
31. J. J. LoTurco, D. F. Owens, M. J. S. Heath, M. B. E. Davis, A. R. Kriegstein, GABA and glutamate depolarize cortical progenitor cells and inhibit DNA synthesis. *Neuron* **15**, 1287–1298 (1995).
32. T. N. Behar, Y. X. Li, H. T. Tran, W. Ma, V. Dunlap, C. Scott, J. L. Barker, GABA stimulates chemotaxis and chemokinesis of embryonic cortical neurons via calcium-dependent mechanisms. *J. Neurosci.* **16**, 1808–1818 (1996).

33. B. Belhage, G. H. Hansen, L. Elster, A. Schousboe, Effects of γ-aminobutyric acid (GABA) on synaptogenesis and synaptic function. *Perspect. Dev. Neurobiol.* **5**, 235–246 (1998).
34. Y. Ben-Ari, Excitatory actions of gaba during development: The nature of the nurture. *Nat. Rev. Neurosci.* **3**, 728–739 (2002).
35. M. Fagiolini, J.-M. Fritschy, K. Löw, H. Möhler, U. Rudolph, T. K. Hensch, Specific $GABA_A$ circuits for visual cortical plasticity. *Science* **303**, 1681–1683 (2004).
36. G. Barbin, H. Pollard, J. L. Gaïarsa, Y. Ben-Ari, Involvement of $GABA_A$ receptors in the outgrowth of cultured hippocampal neurons. *Neurosci. Lett.* **152**, 150–154 (1993).
37. L. Cancedda, H. Fiumelli, K. Chen, M.-m. Poo, Excitatory GABA action is essential for morphological maturation of cortical neurons in vivo. *J. Neurosci.* **27**, 5224–5235 (2007).
38. J. Chen, A. R. Kriegstein, A GABAergic projection from the zona incerta to cortex promotes cortical neuron development. *Science* **350**, 554–558 (2015).
39. S. Z. Young, M. M. Taylor, S. Wu, Y. Ikeda-Matsuo, C. Kubera, A. Bordey, NKCC1 knockdown decreases neuron production through $GABA_A$-regulated neural progenitor proliferation and delays dendrite development. *J. Neurosci.* **32**, 13630–13638 (2012).
40. C. Porcher, I. Medina, J.-L. Gaiarsa, Mechanism of BDNF modulation in GABAergic synaptic transmission in healthy and disease brains. *Front. Cell. Neurosci.* **12**, 273 (2018).
41. B. Riffault, N. Kourdougli, C. Dumon, N. Ferrand, E. Buhler, F. Schaller, C. Chambon, C. Rivera, J.-L. Gaiarsa, C. Porcher, Pro-brain-derived neurotrophic factor (proBDNF)-mediated $p75^{NTR}$ activation promotes depolarizing actions of GABA and increases susceptibility to epileptic seizures. *Cereb. Cortex* **28**, 510–527 (2018).
42. D. D. Wang, A. R. Kriegstein, Blocking early GABA depolarization with bumetanide results in permanent alterations in cortical circuits and sensorimotor gating deficits. *Cereb. Cortex* **21**, 574–587 (2011).
43. H. Lagercrantz, T. A. Slotkin, The "stress" of being born. *Sci. Am.* **254**, 100–107 (1986).
44. J. Maguire, Stress-induced plasticity of GABAergic inhibition. *Front. Cell. Neurosci.* **8**, 157 (2014).
45. Y. Gao, J.-J. Zhou, Y. Zhu, T. Kosten, D.-P. Li, Chronic unpredictable mild stress induces loss of GABA inhibition in corticotrophin-releasing hormone-expressing neurons through NKCC1 upregulation. *Neuroendocrinology* **104**, 194–208 (2017).
46. T. Toda, D. Homma, H. Tokuoka, I. Hayakawa, Y. Sugimoto, H. Ichinose, H. Kawasaki, Birth regulates the initiation of sensory map formation through serotonin signaling. *Dev. Cell* **27**, 32–46 (2013).
47. T. Toda, H. Kawasaki, The development of suckling behavior of neonatal mice is regulated by birth. *Mol. Brain* **7**, 8 (2014).
48. N. Korogod, C. C. Petersen, G. W. Knott, Ultrastructural analysis of adult mouse neocortex comparing aldehyde perfusion with cryo fixation. *eLife* **4**, e05793 (2015).
49. A. E. de Guzman, M. D. Wong, J. A. Gleave, B. J. Nieman, Variations in post-perfusion immersion fixation and storage alter MRI measurements of mouse brain morphometry. *Neuroimage* **142**, 687–695 (2016).
50. N. Ishizuka, W. M. Cowan, D. G. Amaral, A quantitative analysis of the dendritic organization of pyramidal cells in the rat hippocampus. *J. Comp. Neurol.* **362**, 17–45 (1995).
51. J. B. Angevine Jr., Time of neuron origin in the hippocampal region: An autoradiographic study in the mouse. *Exp. Neurol. Suppl.* **2**, 1–70 (1965).
52. J. M. Fitch, J. M. Juraska, L. W. Washington, The dendritic morphology of pyramidal neurons in the rat hippocampal CA3 area. I. Cell types. *Brain Res.* **479**, 105–114 (1989).
53. M. Belle, D. Godefroy, G. Couly, S. A. Malone, F. Collier, P. Giacobini, A. Chédotal, Tridimensional visualization and analysis of early human development. *Cell* **169**, 161–173.e12 (2017).
54. N. Lozovaya, S. Eftekhari, R. Cloarec, L.-A. Gouty-Colomer, A. Dufour, B. Riffault, M. Billon-Grand, A. Pons-Bennaceur, N. Oumar, N. Burnashev, Y. Ben-Ari, C. Hammond, GABAergic inhibition in dual-transmission cholinergic and GABAergic striatal interneurons is abolished in Parkinson disease. *Nat. Commun.* **9**, 1422 (2018).
55. E. S. Lein, M. J. Hawrylycz, N. Ao, M. Ayres, A. Bensinger, A. Bernard, A. F. Boe, M. S. Boguski, K. S. Brockway, E. J. Byrnes, L. Chen, L. Chen, T.-M. Chen, M. C. Chin, J. Chong, B. E. Crook, A. Czaplinska, C. N. Dang, S. Datta, N. R. Dee, A. L. Desaki, T. Desta, E. Diep, T. A. Dolbeare, M. J. Donelan, H.-W. Dong, J. G. Dougherty, B. J. Duncan, A. J. Ebbert, G. Eichele, L. K. Estin, C. Faber, B. A. Facer, R. Fields, S. R. Fischer, T. P. Fliss, C. Frensley, S. N. Gates, K. J. Glattfelder, K. R. Halverson, M. R. Hart, J. G. Hohmann, M. P. Howell, D. P. Jeung, R. A. Johnson, P. T. Karr, R. Kawal, J. M. Kidney, R. H. Knapik, C. L. Kuan, J. H. Lake, A. R. Laramee, K. D. Larsen, C. Lau, T. A. Lemon, A. J. Liang, Y. Liu, L. T. Luong, J. Michaels, J. J. Morgan, R. J. Morgan, M. T. Mortrud, N. F. Mosqueda, L. L. Ng, R. Ng, G. J. Orta, C. C. Overly, T. H. Pak, S. E. Parry, S. D. Pathak, O. C. Pearson, R. B. Puchalski, Z. L. Riley, H. R. Rockett, S. A. Rowland, J. J. Royall, M. J. Ruiz, N. R. Sarno, K. Schaffnit, N. V. Shapovalova, T. Sivisay, C. R. Slaughterbeck, S. C. Smith, K. A. Smith, B. I. Smith, A. J. Sodt, N. N. Stewart, K.-R. Stumpf, S. M. Sunkin, M. Sutram, A. Tam, C. D. Teemer, C. Thaller, C. L. Thompson, L. R. Varnam, A. Visel, R. M. Whitlock, P. E. Wohnoutka, C. K. Wolkey, V. Y. Wong, M. Wood, M. B. Yaylaoglu, R. C. Young, B. L. Youngstrom, X. F. Yuan, B. Zhang, T. A. Zwingman, A. R. Jones, Genome-wide atlas of gene expression in the adult mouse brain. *Nature* **445**, 168–176 (2007).
56. B. Paniagua, A. Lyall, J.-B. Berger, C. Vachet, R. M. Hamer, S. Woolson, W. Lin, J. Gilmore, M. Styner, Lateral ventricle morphology analysis via mean latitude axis. *Proc. SPIE Int. Soc. Opt. Eng.* **8672**, 2006846 (2013).

Acknowledgments: We are grateful to R. Tyzio, A. Pons-Benaceur, M. Chiesa, V. Tsintsadze, and N. Burnashev for their contributions and M. Billon-Grand for technical support.
Funding: Financial support was provided by Neurochlore and the Fondation Bettencourt Schueller. **Author contributions:** R.C. and B.R. performed the iDISCO experiments, microglia, and volume analyses. A.D. performed the neuron reconstruction and analysis. L.-A.G.-C., C.D., D.G., and N.L. performed the patch experiments. S.E. performed the immunohistochemistry experiments. H.R. and P.B. performed the mathematical analysis. R.C., B.R., A.D., H.R., and P.B. performed the statistical analyses. Y.B.-A. conceived the study, and D.C.F. managed it. R.C., B.R., A.D., and Y.B.-A. wrote the paper. All authors discussed and commented on the manuscript. **Competing interests:** With the exception of P.B., the authors' salaries were provided by Neurochlore, a biotech company dedicated to the development of treatments for children with autism. Y.B.-A., D.C.F., and N.L. are shareholders of Neurochlore, and Y.B.-A. is the CEO of the company. All authors declare that they have no other competing interests. **Data and materials availability:** All data needed to evaluate the conclusions in the paper are present in the paper and/or the Supplementary Materials. Additional data related to this paper may be requested from the authors.

Submitted 8 August 2018
Accepted 10 December 2018
Published 23 January 2019
10.1126/sciadv.aav0394

Citation: R. Cloarec, B. Riffault, A. Dufour, H. Rabiei, L.-A. Gouty-Colomer, C. Dumon, D. Guimond, P. Bonifazi, S. Eftekhari, N. Lozovaya, D. C. Ferrari, Y. Ben-Ari, Pyramidal neuron growth and increased hippocampal volume during labor and birth in autism. *Sci. Adv.* **5**, eaav0394 (2019).